Equation of state of fully ionized electron-ion plasmas. II. Extension to relativistic densities and to the solid phase

Alexander Y. Potekhin[1,*] and Gilles Chabrier[2]

[1]*Ioffe Physical-Technical Institute, 194021 St. Petersburg, Russia*
[2]*Ecole Normale Supérieure de Lyon, CRAL (UMR CNRS No. 5574), 69364 Lyon Cedex 07, France*

The analytic equation of state of nonideal Coulomb plasmas consisting of pointlike ions immersed in a polarizable electron background [G. Chabrier and A. Y. Potekhin, Phys. Rev. E **58**, 4941 (1998)] is improved, and its applicability range is considerably extended. First, the fit of the electron screening contribution in the free energy of the Coulomb liquid is refined at high densities where the electrons are relativistic. Second, we calculate the screening contribution for the Coulomb solid (bcc and fcc) and derive an analytic fitting expression. Third, we propose a simple approximation to the internal and free energy of the liquid one-component plasma of ions, accurate within the numerical errors of the most recent Monte Carlo simulations. We obtain an updated value of the coupling parameter at the solid-liquid phase transition for the one-component plasma: $\Gamma_m = 175.0 \pm 0.4(1\sigma)$.

I. INTRODUCTION

Fully ionized electron-ion plasmas (EIP) are encountered in laboratory experiments, in stellar and planetary interiors, in supernova explosions, etc. From the theoretical point of view, the free energy of fully ionized EIP provides the reference system for models aimed at describing the thermodynamic properties of partially ionized plasmas. Thus the studies of EIP are of both theoretical and practical interest.

In a previous paper [1], we have calculated thermodynamic quantities of Coulomb plasmas consisting of pointlike ions immersed in a compressible, polarizable electron background and devised analytic fitting formulas for these quantities. The calculations were based on a linear-response theory for the ion-electron (ie) interaction, which is valid as long as the typical ie interaction energy $(Ze)^2/2a_0$ (where a_0 is the Bohr radius and Ze is the ion charge) is smaller than the kinetic energy of the electrons. This condition is fulfilled either at temperatures $T \gtrsim 10^5 Z^2$ K or at densities $\rho \gtrsim AZ^2$ g cm^{-3}, where A is the ion mass number. For the nonrelativistic regime, i.e., at densities $\rho \ll 10^6$ g cm^{-3}, finite-temperature effects were included in the electronic dielectric function, as well as the local-field correction arising from electron correlation effects, following the model developed in Ref. [2]. In the relativistic regime, similar calculations were done using the Jancovici [3] dielectric function.

Since the electron screening is weak at high densities, and since the bulk of calculations have been performed using the nonrelativistic model, our fit for the ie contribution was not very accurate at $\rho \gtrsim 10^6$ g cm^{-3}, where the electrons are relativistic. Because of the same weakness of the screening, this inaccuracy in the ie contribution at high ρ did not deteriorate the overall accuracy for the *excess* part of the free energy, which sums up the ion-ion (ii), electron-electron (ee), and ie contributions. There are, however, physical problems which require an accurate evaluation of the ie part even at high densities (an example is mentioned below). In this paper, we present a modification of the analytic formula [1] for the ie free energy that improves significantly the accuracy in the domain of relativistic electrons, keeping unchanged the previous nonrelativistic results.

Second, we calculate the ie part of the free energy for a Coulomb solid, where the ions form either a body-centered-cubic (bcc) or face-centered-cubic (fcc) lattice. The calculation is performed in a perturbation approximation, which is accurate because the screening is weak. We employ an analytic expression for the ion structure factor $S(k)$ of a Coulomb crystal, obtained in Ref. [4] in the harmonic approximation for large wave numbers k outside the first Brillouin zone. For small k, we supplement it by an exact limiting form of $S(k)$. We evaluate the screening contribution for both the classical and quantum harmonic crystals and construct a fitting formula which accurately reproduces our numerical results.

The above-mentioned improvements of the equation of state are significant at densities $\rho \gtrsim 10^6$ g cm^{-3}. Such densities cannot be reached in the laboratory, but they are commonly encountered in the interiors of white dwarfs and envelopes of neutron stars (e.g., Ref. [5]).

In addition, we present simple formulas for the excess internal and free energies of a classical one-component plasma (OCP) liquid, which take into account the most recent Monte Carlo (MC) results [6,7], and which are accurate for any values of the Coulomb coupling parameter from the gaseous phase to the dense liquid regime. Analyzing various results for the free energy of the OCP liquid and solid, we revise the value of the coupling parameter at the solid-liquid phase transition.

In the next section, we describe the basic parameters of the EIP. In Sec. III, we consider the OCP liquid and determine its freezing point. In Sec. IV, we present an improved fit to the free-energy contribution due to the electron screening in a Coulomb liquid. In Sec. V, we evaluate an analogous

*Electronic address: palex@astro.ioffe.rssi.ru

contribution for a Coulomb solid and fit it by an analytic expression.

II. THERMODYNAMIC PARAMETERS

We consider EIP consisting of pointlike ions and electrons. The basic dimensionless parameters are the electron density parameter r_s and the ion coupling parameter Γ:

$$r_s = \frac{a_e}{a_0}, \quad \Gamma = \frac{(Ze)^2}{k_B Ta} = \Gamma_e Z^{5/3}, \quad \Gamma_e = \frac{e^2}{k_B Ta_e}. \quad (1)$$

Here, k_B is the Boltzmann constant, $a_e = (\frac{4}{3}\pi n_e)^{-1/3}$ is the mean interelectron distance, $a = (\frac{4}{3}\pi n_i)^{-1/3} = a_e Z^{1/3}$ is the mean interion distance, and $n_e(n_i)$ denotes the electron (ion) number density. Γ_e denotes the coupling parameter for nondegenerate electrons.

Quantization of the ionic motion is important if $T \ll T_p = \hbar\omega_p/k_B$, where $\omega_p = (4\pi Z^2 e^2 n_i/m_i)^{1/2}$ is the ion plasma frequency, m_i being the ion mass. A corresponding dimensionless parameter is

$$\eta = T_p/T = \Gamma\sqrt{3/R_S}, \quad (2)$$

where

$$R_S = \frac{am_i}{\hbar^2}(Ze)^2 = \frac{m_i}{m_e} r_s Z^{7/3} \quad (3)$$

is the ion density parameter. We neglect ion quantum-exchange effects, which is justified if $R_S \gg \Gamma$ (see, e.g., Ref. [8]).

The electrons are characterized by the degeneracy parameter θ and the relativity parameter x_r,

$$\theta = T/T_F, \quad x_r = p_F/(m_e c), \quad (4)$$

where T_F is the Fermi temperature, c is the speed of light, and $p_F = \hbar(3\pi^2 n_e)^{1/3}$ is the Fermi momentum. The electron screening properties are determined by the Thomas-Fermi wave number

$$k_{\text{TF}} = (4\pi e^2 \partial n_e/\partial\mu)^{1/2}, \quad (5)$$

where μ is the electron chemical potential.

For these parameters, the following estimates are accurate within 0.005%:

$$x_r \approx 0.014\,005 r_s^{-1} \approx 1.0088(\rho_6 Z/A)^{1/3}, \quad (6)$$

$$\Gamma_e \approx \frac{22.547 x_r}{T_6}, \quad \theta^{-1} \approx \frac{5930}{T_6}(\sqrt{1+x_r^2}-1), \quad (7)$$

where $\rho_6 = \rho/(10^6 \text{ g cm}^{-3})$ and $T_6 = T/(10^6 \text{ K})$. In the nonrelativistic plasma ($x_r \ll 1$), $\theta \approx 0.543 r_s/\Gamma_e$. In the ultrarelativistic case ($x_r \gg 1$), $\theta \approx (263\Gamma_e)^{-1}$. If the electrons are nondegenerate ($\theta \gg 1$), $k_{\text{TF}} a_e \approx \sqrt{3\Gamma_e}$. For strongly degenerate electrons ($\theta \ll 1$),

$$k_{\text{TF}} a_e \approx 0.185(1+x_r^{-2})^{1/4}. \quad (8)$$

The ion quantum parameter η is expressed through x_r and Γ as

$$\eta \approx 0.3428\Gamma\sqrt{x_r}Z^{-7/6}A^{-1/2}. \quad (9)$$

Within the aforementioned approximation of weak electron-ion coupling, the total Helmholtz free energy F_{tot} can be written as

$$F_{\text{tot}} = F_{\text{id}}^{(i)} + F_{\text{id}}^{(e)} + F_{ee} + F_{ii} + F_{ie}, \quad (10)$$

where $F_{\text{id}}^{(i,e)}$ denote the ideal free energy of ions and electrons, respectively, and the last three terms represent an excess free energy arising from interactions. $F_{\text{id}}^{(i)}$ is the free energy of an ideal Boltzmann gas. For the electrons at arbitrary degeneracy and relativism, $F_{\text{id}}^{(e)}$ can be expressed through Fermi-Dirac integrals and approximated by analytic formulas [1]. An analytic parametrization for the nonideal (exchange and correlation) part of the free energy of the nonrelativistic electrons, F_{ee}^{nr}, has been given in Ref. [9]. For the relativistic electrons, the exchange free energy F_x^{rel} has been given, e.g., in Ref. [10], while the correlation corrections are negligible because they contain an additional small factor $\sim \alpha_f \ln|\alpha_f|$ [11], where $\alpha_f \approx 1/137$ is the fine-structure constant. In practice, we use the following interpolation between the nonrelativistic and relativistic regimes: if $\Gamma_e \geq 0.07$ and $r_s \leq 0.13$, we set

$$F_{ee} = (1-\xi)F_{ee}^{\text{nr}} + \xi F_x^{\text{rel}},$$
$$\xi = \exp[-(\Gamma_e/0.07-0.9)^{-2} - (0.13/r_s-0.9)^{-2}]; \quad (11)$$

otherwise we set $F_{ee} = F_{ee}^{\text{nr}}$. The interpolation is sufficiently smooth, because F_{ee}^{nr} and F_x^{rel} closely match each other at the chosen boundary between the two regimes.

In the following sections, we consider the last two terms in Eq. (10), which represent the excess free energy of an OCP of ions and the contribution due to the ion-electron interactions, respectively.

III. OCP AND MELTING TRANSITION

Liquid and solid phases of the OCP have been studied extensively by various analytic and numerical methods. All the thermodynamic functions of the classical OCP can be expressed as functions of the only parameter Γ. At $\Gamma \ll 1$, a diagrammatic cluster expansion yields

$$u_{ii} \equiv \frac{U_{ii}}{N_i k_B T} = -\sqrt{\frac{3}{2}}\Gamma^{3/2} - 3\Gamma^3\left[\frac{3}{8}\ln(3\Gamma) + \frac{C_E}{2} - \frac{1}{3}\right]$$
$$- \Gamma^{9/2}(1.6875\sqrt{3}\ln\Gamma - 0.235\,11) + \cdots, \quad (12)$$

where $C_E = 0.577\,21\ldots$ is the Euler constant. Here, the first term is the Debye-Hückel energy, the second one is due to Abe [12], and the $\sim\Gamma^{9/2}$ one is due to Cohen and Murphy [13]. Since F_{ii} vanishes at high T, it can be obtained from U_{ii} by integration:

$$f_{ii} \equiv \frac{F_{ii}}{N_i k_B T} = \int_0^\Gamma \frac{u_{ii}(\Gamma')}{\Gamma'}d\Gamma' \quad (13)$$

TABLE I. Parameters of Eq. (15). Powers of 10 are given in square brackets.

Data	$-A_1$	A_2	B_1	B_2	$-B_3$	B_4
Ref. [6]	0.9070	0.62954	4.56[−3]	211.6	1.0[−4]	4.62[−3]
Ref. [7]	0.907347	0.62849	4.50[−3]	170.0	8.4[−5]	3.70[−3]

$$= -\frac{\Gamma^{3/2}}{\sqrt{3}} - \Gamma^3\left(\tfrac{3}{8}\ln\Gamma + 0.242\,25\right)$$

$$- \Gamma^{9/2}(0.649\,52\ln\Gamma - 0.196\,58) + \cdots. \quad (14)$$

The above analytic expansion is not applicable for $\Gamma \gtrsim 1$. The most accurate up to date numerical results for the internal energy of the liquid OCP at $1 \lesssim \Gamma \lesssim 200$ have been obtained by MC simulations by DeWitt and Slattery [6] and by Caillol [7]. These authors have also constructed analytic fits to their data with the standard deviations comparable to the numerical MC noise. Unfortunately, these fits cannot be extended to small Γ, which hampers obtaining the free energy by Eq. (13). On the other hand, the hypernetted-chain (HNC) result for F_{ii} at $\Gamma = 1$ is slightly inaccurate because the HNC approximation neglects the so-called bridge functions in the diagrammatic representation of the interactions. To circumvent the difficulty, DeWitt and Slattery [14] used small differences between HNC and MC at $\Gamma = 0.8$ and 0.6 to get the corrected value of $f_{ii}(\Gamma = 1) = -0.4368$.

We propose a different approach. We consider the parametrization

$$u_{ii} = \Gamma^{3/2}\left[\frac{A_1}{\sqrt{\Gamma + A_2}} + \frac{A_3}{\Gamma + 1}\right] + \frac{B_1\Gamma^2}{\Gamma + B_2} + \frac{B_3\Gamma^2}{\Gamma^2 + B_4}, \quad (15)$$

where $A_3 = -\sqrt{3}/2 - A_1/\sqrt{A_2}$. The terms in square brackets have been used in Ref. [1], the term with B_1 provides an adjustment of the fit to the MC data at large Γ, and the last term adjusts to Eq. (12) at small Γ. The best-fit parameters with respect to the data [6,7] are given in Table I. Then the free energy can be obtained from Eq. (13):

$$f_{ii} = A_1\left[\sqrt{\Gamma(A_2 + \Gamma)} - A_2\ln\left(\sqrt{\Gamma/A_2} + \sqrt{1 + \Gamma/A_2}\right)\right]$$

$$+ 2A_3\left[\sqrt{\Gamma} - \arctan\sqrt{\Gamma}\right] + B_1\left[\Gamma - B_2\ln\left(1 + \frac{\Gamma}{B_1}\right)\right]$$

$$+ \frac{B_3}{2}\ln\left(1 + \frac{\Gamma^2}{B_4}\right). \quad (16)$$

The corresponding expression for heat capacity is

$$\frac{C_{V,ii}}{N_i k_B} = \frac{\Gamma^{3/2}}{2}\left[A_3\frac{\Gamma - 1}{(\Gamma + 1)^2} - \frac{A_1 A_2}{(\Gamma + A_2)^{3/2}}\right] + \Gamma^2\left[B_3\frac{\Gamma^2 - B_4}{(\Gamma^2 + B_4)^2}\right]$$

$$- \frac{B_1 B_2}{(\Gamma + B_2)^2}\right]. \quad (17)$$

Comparison of Eq. (15) with Eq. (12) at $\Gamma < 1$ and with the MC data from Refs. [6,7] at $\Gamma \gtrsim 1$, supplemented by some of our HNC calculations, is given in Fig. 1. The upper
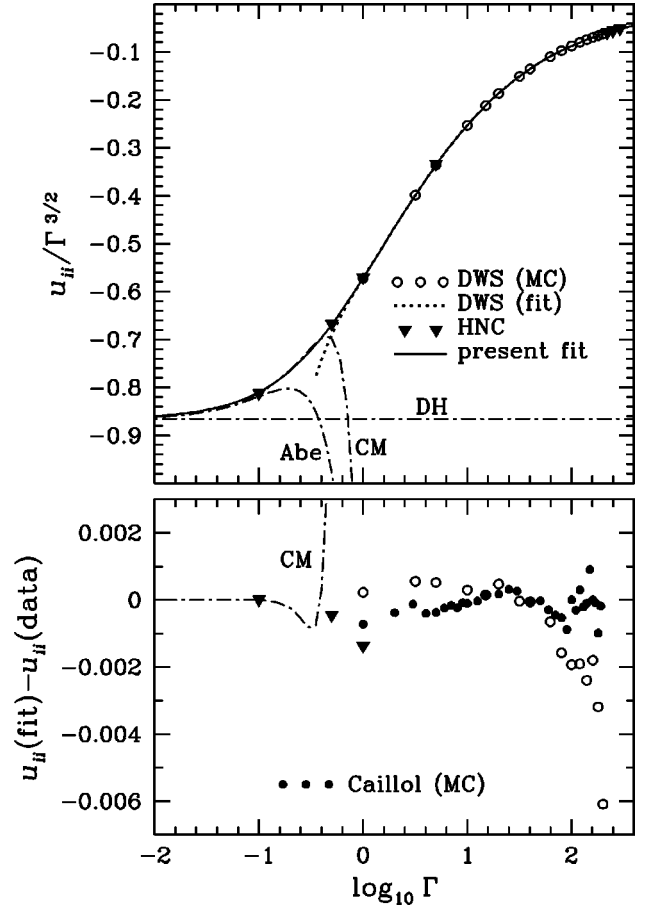

FIG. 1. Upper panel: comparison of the fit (15) (solid line) with the Debye-Hückel (DH), Abe [12], and Cohen-Murphy [13] (CM) approximations (dot-dashed lines), with the MC results (circles) and the fit (dotted line) of Ref. [6] (DWS), and with some of our HNC results (triangles). Lower panel: residual differences between the fit (15) and (i) the analytic expansion (12) (dot-dashed line), (ii) results of HNC calculations (triangles), (iii) MC results of Ref. [6] (open circles), and (iv) numerical results of Ref. [7] (MC+extrapolation).

panel displays the ratio $u_{ii}/\Gamma^{3/2}$ (which is constant in the Debye-Hückel approximation). The magnitude of the possible error is demonstrated by the lower panel. Here, the dot-dashed line shows the difference between the approximation (15) with the second set of parameters and expansion (12), while various symbols show residual differences between the same approximation and numerical (HNC and MC) results. The distribution of the residuals around zero looks irregular, which indicates that they represent numerical noise of the MC calculations rather than an error of the fit (15). In addition, we have checked that the difference between our fit to the free energy, Eq. (16), and the one in Ref. [6] (at $\Gamma \gtrsim 1$), is of the order of the aforementioned small uncertainty in $f_{ii}(\Gamma = 1)$.

More complicated interpolations between the low- and high-Γ limits were proposed previously [15,16]. By construction, they reproduce exactly Eq. (12) at $\Gamma \to 0$ and the fits to MC results at $\Gamma \gtrsim 1$. Compared with the present fit, however, those interpolations have somewhat larger differences from the HNC results at $0.1 < \Gamma < 1$.

The freezing of Coulomb OCP liquid into a bcc crystal occurs when the free energy of the solid becomes lower than
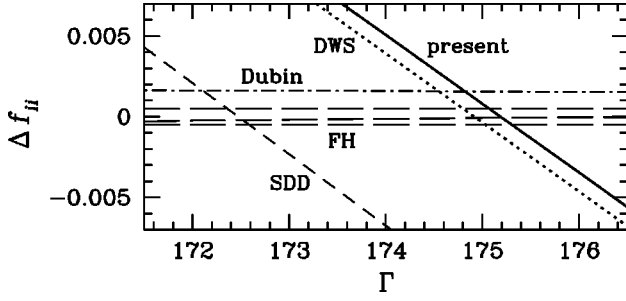
FIG. 2. Difference between the free energy of the solid OCP given by a three-parameter fit of Ref. [20] and parametrizations for the liquid OCP according to Refs. [19] (SDD; short-dashed line), [6] (dotted line), Eq. (16) (solid line), and for the solid according to Dubin [18] (dot-dashed line). The long-dashed lines marked "FH" correspond to the four-parameter fit and to the $\pm 1\sigma$ uncertainty of the three-parameter fit in Ref. [20].

that of the liquid at $\Gamma = \Gamma_m$. Nagara *et al.* [17] and Dubin [18], having improved a previous treatment of anharmonic corrections to the free energy of the Coulomb crystal, obtained $\Gamma_m = 172 \pm 1$. However, these authors employed an older fit [19] (SDD) for the liquid. Figure 2 shows the *differences* between f_{ii} for the solid and liquid OCP given by various parametrizations. For the solid, we have adopted the three-parameter fit by Farouki and Hamaguchi [20] to their molecular-dynamics simulations in the range $170 \le \Gamma \le 400$. The horizontal long-dashed lines correspond to the standard deviation of that fit. The line between them represents a four-parameter fit [20] in the same Γ interval. The dot-dashed line shows the difference between the fit of Ref. [20] and that by Dubin [18]. The value of Γ_m indicated above is given by the intersection of the latter line with the short-dashed one (SDD). Using updated results for the OCP liquid [either Ref. [6] or our Eq. (16), represented by the dotted and solid line, respectively] and the OCP solid [20], we obtain $\Gamma_m = 175.0 \pm 0.4$.

IV. ELECTRON SCREENING IN A COULOMB LIQUID

We now consider electron polarization effects in the EIP. In a previous paper [1], we have calculated F_{ie} using the model developed in Ref. [2] for nonrelativistic EIP. The HNC equations have been solved numerically for an effective screened interion potential V_{eff}, which is the sum of the bare ionic potential and the induced polarization potential, to obtain $F_{ii} + F_{ie}$ and corresponding contributions to the internal energy $(U_{ii} + U_{ie})$ and pressure $(P_{ii} + P_{ie})$. The same equations solved for the bare Coulomb potential give F_{ii}, U_{ii}, and P_{ii}. The difference represents the screening (*ie*) part. Inclusion of the finite-temperature effects in V_{eff} provides a correct treatment of the thermodynamic quantities over a wide range of values of Γ from the Debye-Hückel limit $\Gamma \ll 1$ to the strong-coupling limit $\Gamma \gg 1$ for various r_s and Z.

Relativistic calculations have been performed employing the same HNC technique but with the Jancovici [3] dielectric function $\varepsilon(k, x_r)$, which is appropriate at strong degeneracy $(\theta \ll 1)$ and arbitrary x_r. The results are in good agreement with those obtained by Yakovlev and Shalybkov [11], who have used an equation

$$f_{ie} \equiv \frac{F_{ie}}{N_i k_B T} = -\frac{\Gamma a}{\pi} \int_0^\infty S(k, \Gamma)[\varepsilon(k, x_r) - 1]dk, \quad (18)$$

where $S(k, \Gamma)$ is the static structure factor of ions (i.e., the Fourier transform of the ion radial distribution function). Equation (18) has been derived by Galam and Hansen [21] using a thermodynamic perturbation scheme, which can be represented as an expansion in powers of k_{TF}. We have repeated the calculations [11] using a more recent and accurate $S(k, \Gamma)$ [22] than in the original work; the change in f_{ie} due to this update does not exceed 4%.

Note that Eq. (18) differs from the standard first-order perturbation approximation by a replacement of $[1 - 1/\varepsilon]$ by $[\varepsilon - 1]$. The resulting difference $\approx (k_{\text{TF}}a)^3/6$ has the same order of magnitude as the second-order perturbation correction [21]. Our HNC calculations with the Jancovici dielectric function at $x_r \lesssim 1$ and $\Gamma \gtrsim 1$ coincide within 2% with the results of Ref. [11], whereas the substitution of $[1 - 1/\varepsilon]$ in Eq. (18) yields a considerable difference: for example, for $\Gamma = 1$ and $Z = 26$ this difference approaches 40% even at large x_r. We conclude that the approximation (18) is very accurate at high densities.

The screening contribution to the free energy of the Coulomb liquid at $0 < r_s \lesssim 1$, $0 < \Gamma \lesssim 300$, and $1 \le Z \le 26$ has been fitted by the expression [1]

$$f_{ie} \equiv \frac{F_{ie}}{N_i k_B T} = -\Gamma_e \frac{c_{\text{DH}}\sqrt{\Gamma_e} + c_{\text{TF}}a\Gamma_e^\nu g_1 h_1}{1 + [b\sqrt{\Gamma_e} + a g_2 \Gamma_e^\nu/r_s]h_2}, \quad (19)$$

where $c_{\text{DH}} = (Z/\sqrt{3})[(1+Z)^{3/2} - 1 - Z^{3/2}]$ ensures exact transition to the Debye-Hückel limit at $\Gamma \to 0$, $c_{\text{TF}} = (18/175)(12/\pi)^{2/3}Z^{7/3}(1 - Z^{-1/3} + 0.2 Z^{-1/2})$ reproduces the Thomas-Fermi limit [23] at $Z \to \infty$, the parameters $a = 1.11Z^{0.475}$, $b = 0.2 + 0.078(\ln Z)^2$, and $\nu = 1.16 + 0.08 \ln Z$ provide a low-order approximation to F_{ie} for intermediate r_s and Γ, and the functions

$$g_1 = 1 + 0.78[21 + \Gamma_e(Z/r_s)^3]^{-1}(\Gamma_e/Z)^{1/2},$$

$$g_2 = 1 + \frac{Z-1}{9}\left(1 + \frac{1}{0.001Z^2 + 2\Gamma_e}\right)\frac{r_s^3}{1 + 6r_s^2}$$

improve the fit at relatively large r_s. The results of our non-relativistic finite-temperature HNC calculations are reproduced by setting h_1 and h_2 equal to unity; these factors come into play in the relativistic case.

In the latter case, the asymptotic behavior of Eq. (19) at $\Gamma \to \infty$ should change from $f_{ie} \propto \Gamma r_s$ to $f_{ie} \propto \Gamma r_s \sqrt{1 + x_r^2}$. This is achieved simply by setting $h_2 = (1 + x_r^2)^{-1/2}$. Then the zero-temperature Thomas-Fermi limit [23] $(r_s \ll 1, \Gamma \to \infty, Z \to \infty)$ is reproduced exactly.

The factor h_1 is devised to correct the fit at finite Z in the relativistic domain. A form chosen previously [1] was not very accurate, as illustrated by the dotted lines in Fig. 3 for the internal energy

$$u_{ie} \equiv U_{ie}/(N_i k_B T) = \partial f_{ie}(r_s, \Gamma)/\partial \ln \Gamma. \quad (20)$$

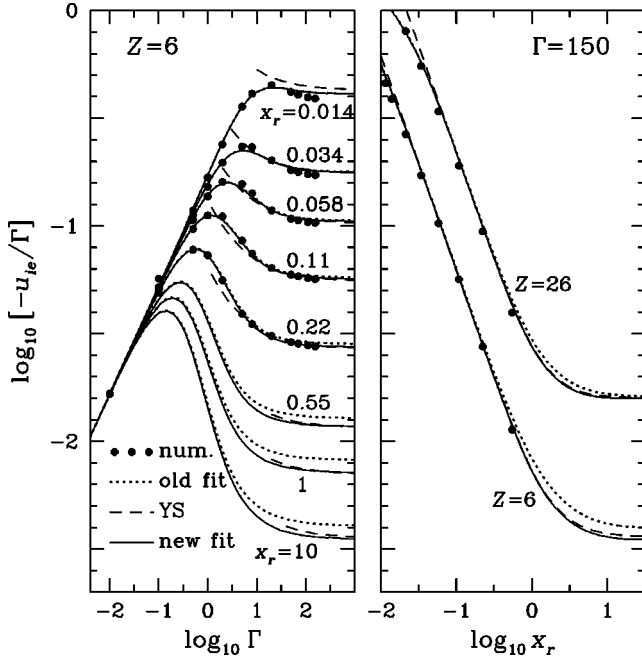A more accurate relativistic correction reads

FIG. 3. Calculated (filled circles) and fitted (solid lines) normalized contribution to the internal energy due to polarization, u_{ie}, as a function of Γ at different values of x_r, $Z=6$ (left panel) and as function of x_r at two values of Z, $\Gamma=150$ (right panel). For comparison, approximations [1] (dotted lines) and [11] (dashed lines) are also shown.

$$h_1(x_r) = \frac{1+x_r^2/5}{1+0.18Z^{-1/4}x_r+0.37Z^{-1/2}x_r^2+x_r^2/5}. \quad (21)$$

The resulting u_{ie} [Eq. (20)] is plotted by the solid lines in Fig. 3. There is now a good agreement with the thermodynamic perturbation expansion [11] at large Γ for any x_r, without deteriorating the accuracy of the old fit in the non-relativistic domain. Quantitatively, for $1<\Gamma<100$ and $x_r<0.25$, the difference between the fit and the HNC results is typically 2–3 %, with a maximum 8% for $Z=1$, $\Gamma=100$, and $r_s=2.074$ (the maximum r_s value used in the calculations). Note that the model of EIP has only marginal physical relevance at such large values of r_s and Γ because of the incipient bound-state formation. On the other hand, at very strong coupling ($\Gamma \gtrsim 100$) and relativistic densities ($x_r > 0.1$), the results of Ref. [11] and of our relativistic HNC calculations are reproduced by our fit with typical deviation of 1–3 % (maximum 4.3% at $Z=6$, $\Gamma=100$, and $x_r=10$).

The heat capacity per ion in units of k_B, C_V/N_ik_B, of the classical EIP liquid is shown in Fig. 4 for $Z=6$ and $T=10^6$, and 10^7 K. These plasma conditions can occur, for example, in interiors of some giant stars or in accreted envelopes of neutron stars [24]. Various contributions, shown in the figure, correspond to separate terms in Eq. (10). At relatively low densities, the main contribution is that of the electrons, with the limiting value $\frac{3}{2}Z=9$. With increasing ρ, the electron gas becomes degenerate, and its heat capacity decreases. Then C_V is determined by the ion liquid. The Coulomb (ii) contribution slightly exceeds the kinetic one ($\frac{3}{2}$) near freezing. According to the equipartition theorem, in a classical ionic crystal the potential and kinetic contributions
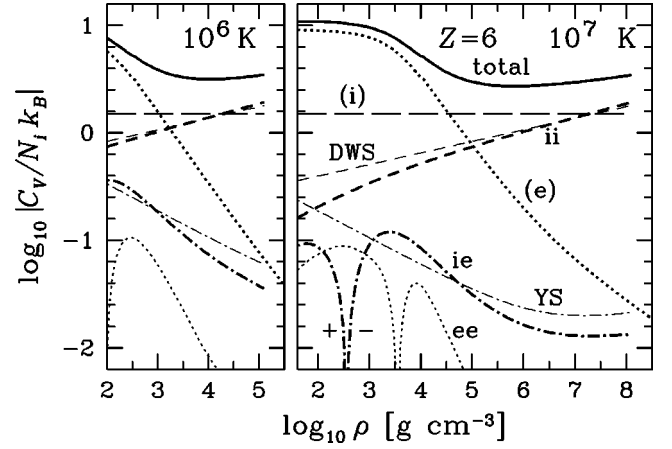

FIG. 4. Absolute values of the heat capacity of fully ionized liquid carbon at $T=10^6$ K and 10^7 K. Dotted curves show the contributions of the electrons (heavy line, ideal Fermi-gas contribution; light line, exchange and correlation correction); dashed lines, contributions of the ions (long dashes, ideal-gas part; short dashes, correlation part); and dot-dashed curves, ion-electron (polarization) correction. The latter curves end at $\Gamma=175$. The dips on the ee and ie curves signify a change of sign. For the ii and ie contributions, present approximations (heavy lines) are compared with those in Refs. [6] (DWS) and [11] (YS) (light lines). The heavy solid line shows the sum of all terms.

are each equal to $\frac{3}{2}$ (apart from small anharmonic corrections). This means that freezing is accompanied by a drop of C_V, equal to the excess of the potential contribution over the kinetic one in the ionic liquid just before freezing. We see, however, that this excess (and hence the drop) is not large.

The values of $C_{V,ii}$ determined by Eq. (17) (thick dashes) and derived from the fit in Ref. [6] (thin dashes) are close to each other near freezing. With decreasing density, however, a large difference develops, which is natural because the formula in Ref. [6] is not applicable at small Γ. Of the same origin is the striking discrepancy between the approximations for $C_{V,ie}$ derived from Eq. (19) (thick dot-dashed curve) and from the fit in Ref. [11] (YS), seen at low ρ. In this domain, our fit describes the change of sign of $C_{V,ie}$ from negative in the strong-coupling regime to positive in the Debye-Hückel domain. However, an appreciable difference with Ref. [11] persists even at large ρ, where both fits describe f_{ie} equally well (within uncertainties in the structure factor). This reflects insufficient accuracy of the present-day determination of the functional form of $S(k,\Gamma)$ for the strongly coupled Coulomb liquid.

V. ELECTRON SCREENING IN A COULOMB SOLID

A. Perturbation approximation

At high densities and below a certain temperature, the ionic Coulomb plasma forms a Wigner crystal. For example, interiors of cool white dwarfs [25] are expected to be in the solid state. The cooling is governed essentially by the compressibility and heat capacity of their interiors, whose central regions are compressed to relativistic densities. In that case, the main contributions to the internal energy (the zero-temperature electron-gas kinetic energy and the ion electrostatic part) do not depend on temperature, so that the heat

capacity is entirely determined by small temperature-dependent corrections. Therefore, evaluation of the polarization corrections for the Coulomb solid is important for astrophysical applications.

Since the maximum ion frequency in the solid is quite small compared to the electron plasma frequency, one can use the adiabatic (i.e., Born-Oppenheimer) approximation, which allows us to decouple the electron and ion dynamics. Even so, a calculation of the thermodynamic functions of a Coulomb solid with allowance for the *ie* interactions is a complex problem. A rigorous treatment would consist in calculating the dynamical matrix and solving a corresponding dispersion relation for the phonon spectrum. The first-order perturbation approximation for the dynamical matrix of a classical Coulomb solid with the polarization corrections, based on an *effective* interion potential, was derived by Pollock and Hansen [26]. In a quantum crystal, strictly speaking, one would have to consider the electron-phonon interactions, in order to calculate the perturbed spectrum.

As mentioned above, the polarization of the electron gas is weak at the high densities in which we are interested. This suggests a simpler, semiclassical perturbation approach to evaluate the polarization corrections. The ionic crystal without *ie* interactions is a natural reference model. Note that the effective interion potential in the adiabatic perturbation approximation [26] is just the electrostatic potential, common to the liquid and solid phases. The difference of this potential from the bare Coulomb potential can be considered as perturbation. Then we can apply the Galam-Hansen [21] perturbation theory, which is based on the *exact* expression for the free energy involving an integration over a coupling parameter related to the ''strength'' of the perturbation. Thus we recover Eq. (18) in the case of a solid, with $S(k)$ replaced by $(4\pi)^{-1}\int S(\mathbf{k})d\Omega$, where $d\Omega$ is a solid angle element in the direction of $\mathbf{k}$.

The resulting polarization correction (18) does not take into account quantum aspects of the *ie* (electron-phonon) interactions, but it allows us to study effects arising from quantum modifications of the ion-ion correlations. These correlations are described by the structure factor S, which depends in this case on $\mathbf{k}$, Γ, and η.

B. Structure factor

In a crystal, the static structure factor is given by

$$S(\mathbf{k},\Gamma,\eta)=\frac{1}{N_i}\sum_{i,j} e^{i\mathbf{k}\cdot(\mathbf{R}_i-\mathbf{R}_j)}\langle e^{i\mathbf{k}\cdot\hat{\mathbf{u}}_i}e^{-i\mathbf{k}\cdot\hat{\mathbf{u}}_j}\rangle_T, \quad (22)$$

where $\hat{\mathbf{u}}_i$ is an operator of ion displacement from an equilibrium lattice position $\mathbf{R}_i$, and $\langle\cdots\rangle_T$ denotes the canonical average. The structure factor (22) can be decomposed into elastic (or static-lattice) and inelastic parts,

$$S(\mathbf{k},\Gamma,\eta)=S'(\mathbf{k},\Gamma,\eta)+S''(\mathbf{k},\Gamma,\eta). \quad (23)$$

The elastic part is (e.g., Ref. [27])

$$S'_{\text{sol}}(\mathbf{k},\Gamma,\eta)=(2\pi)^3 n_i e^{-2W(\mathbf{k},\Gamma,\eta)}\sum_{\mathbf{G}}{}'\,\delta(\mathbf{k}-\mathbf{G}), \quad (24)$$

TABLE II. Parameters of Coulomb crystals [33].

Lattice type	μ_{-2}	μ_{-1}	μ_1	C_M
bcc	12.973	2.798 55	0.511 3875	0.895 929 255 682
fcc	12.143	2.719 82	0.513 1940	0.895 873 615 195

where $\Sigma'_{\mathbf{G}}$ denotes a summation over all reciprocal-lattice vectors $\mathbf{G}$ but $\mathbf{G}=0$, and $e^{-2W}\equiv\langle\exp(i\mathbf{k}\cdot\hat{\mathbf{u}})\rangle^2_T$ is the Debye-Waller factor. In isotropic (e.g., cubic) crystals, one has

$$2W(\mathbf{k},\Gamma,\eta)=r_T^2(\Gamma,\eta)k^2/3, \quad (25)$$

where $r_T^2=\langle\hat{\mathbf{u}}^2\rangle_T$ is the mean-squared ion displacement (cf. [27]). In a harmonic crystal,

$$r_T^2=\frac{a^2\eta}{\Gamma}\left[\frac{\mu_{-1}}{2}+\left\langle\frac{\omega_p}{\omega_\nu}\frac{1}{\exp(\hbar\omega_\nu/k_BT)-1}\right\rangle_{\text{ph}}\right], \quad (26)$$

where $\nu\equiv(\mathbf{q},s)$, $s=1,2,3$ enumerates phonon modes, $\mathbf{q}$ is a phonon wave vector, ω_ν is the frequency, $\langle\cdots\rangle_{\text{ph}}$ denotes averaging over phonon wave vectors and polarizations, and $\mu_n\equiv\langle(\omega_\nu/\omega_p)^n\rangle_{\text{ph}}$. In the classical limit ($\eta\to0$), $r_T^2=\mu_{-2}a^2/\Gamma$; and in the quantum limit ($\eta\to\infty$), $r_T^2\sim\mu_{-1}a^2\eta/(2\Gamma)$. Numerical values of μ_{-1} and μ_{-2} are given in Table II. At arbitrary η, a convenient analytic approximation to r_T^2 is provided by a model of the harmonic Coulomb crystal [28], which treats two acoustic modes as degenerate Debye modes with $\omega_\nu=\alpha\omega_p q/q_{\text{BZ}}$, where $q_{\text{BZ}}=(6\pi^2 n_i)^{1/3}$ is the equivalent radius of the Brillouin zone, and the longitudinal mode is an Einstein mode with $\omega_\nu=\gamma\omega_p$. Accuracy of this model for the thermodynamics of the bcc Coulomb crystal has been demonstrated in Ref. [29], where the values $\alpha=0.399$ and $\gamma=0.899$ have been derived from the requirement that the model should reproduce the exact values of μ_{-2} and $\mu_2=\frac{1}{3}$. For the fcc lattice, we obtain $\alpha=0.413$ and $\gamma=0.892$. Using this model, we can calculate the second term in Eq. (26), which yields

$$r_T^2=\frac{a^2}{\Gamma}\left[\frac{\mu_{-1}\eta}{2}+\frac{\eta}{3\gamma(e^{\gamma\eta}-1)}+\frac{2}{\alpha^3\eta}\int_0^{\alpha\eta}\frac{tdt}{e^t-1}\right]. \quad (27)$$

This approximation ensures the correct classical and quantum limits. Between these limits, the maximum deviation from accurate numerical results [33] reaches 1.6% at $\eta\approx9$ for both bcc and fcc lattices.

According to Eq. (23), Eq. (18) can be rewritten as

$$f_{ie}=f'_{ie}+f''_{ie}, \quad (28)$$

$$f'_{ie}=-\frac{3\Gamma}{2}\sum_{\mathbf{G}}{}'\,\frac{\varepsilon(G,x_r)-1}{(Ga)^2}\exp[-2W(G,\Gamma,\eta)], \quad (29)$$

$$f''_{ie}=-\frac{\Gamma a}{\pi}\int_0^\infty S''(k,\Gamma,\eta)[\varepsilon(k,x_r)-1]dk. \quad (30)$$

The inelastic part of the structure factor of a harmonic crystal reads [4]

$$S'' = e^{-2W} \sum_{\mathbf{R}} e^{i\mathbf{k}\cdot\mathbf{R}} [e^{v(\mathbf{R})k^2} - 1], \tag{31}$$

$$v(R) = \frac{3\hbar}{2m_i} \left\langle \frac{(\mathbf{k}\cdot\mathbf{e}_\nu)^2}{k^2} \frac{\cos(\mathbf{q}\cdot\mathbf{R})}{\omega_\nu \tanh(\hbar\omega_\nu/2k_BT)} \right\rangle_{ph} \tag{32}$$

(where $\mathbf{e}_\nu$ is a phonon polarization vector). A straightforward use of this expression is impractical because of a slow convergence of the sum. For this reason, we employ the approximation [4]

$$S''(k,\Gamma,\eta) \approx S_0''(k,\Gamma,\eta) \equiv 1 - \exp[-2W(k,\Gamma,\eta)]. \tag{33}$$

As argued in Ref. [4], this approximation is good for use in integrals over $\mathbf{k}$ at $k > q_{BZ}$. In papers addressed to the transport properties of Coulomb plasmas [4,30], integrals over k were truncated from below at $k = q_{BZ}$. In Eq. (30), however, it is essential to recover the correct limiting behavior of $S''(k)$ at $k \to 0$, since $[\varepsilon - 1] \propto k^{-2}$ becomes large in this limit. Therefore, we use a piecewise approximation:

$$S'' = \begin{cases} S_0'' & (k \geq k_1), \\ S_1'' \equiv \frac{1}{2} k^2 [\partial^2 S''/\partial k^2]_{k\to 0} & (k < k_1), \end{cases} \tag{34}$$

where the parameter k_1 will be determined below. The exact result for classical Coulomb plasmas [31] reads $S_1''(k) = (ka)^2/(3\Gamma)$. In a general case, $S_1''(k)$ can be found from Eq. (31). At small k, the expression in the square brackets in Eq. (31) can be replaced by $v(\mathbf{R})k^2$, which corresponds to the one-phonon approximation. Changing the order of averaging and summation, we see that the summation yields delta function $\delta(\mathbf{k}\pm\mathbf{q}-\mathbf{G})$; therefore, $\mathbf{q} = \pm\mathbf{k}$ as long as $k < \min G \approx 2q_{BZ}$. Hence, only the longitudinal phonon mode contributes in this limit. The frequency of this mode in a Coulomb crystal tends to ω_p at small q (e.g., [26]), which enables us to perform averaging in Eq. (32). Finally, we obtain

$$S_1''(k,\Gamma,\eta) = \frac{(ka)^2}{6\Gamma} \frac{\eta}{\tanh(\eta/2)}. \tag{35}$$

In order to test our approximation (34) and to find the optimum value of k_1, let us consider the electrostatic energy $U_{el\text{-}st}$ of a Coulomb crystal,

$$u_{el\text{-}st} \equiv \frac{U_{el\text{-}st}}{N_i k_B T} = \frac{\Gamma a}{\pi} \int_0^\infty [S(k) - 1] dk = u' + u'', \tag{36}$$

where, according to Eqs. (23) and (24),

$$u' = \frac{3\Gamma}{2} \sum_{\mathbf{G}}' \frac{e^{-2W(G,\Gamma,\eta)}}{(Ga)^2} \tag{37}$$

is the static-lattice part. Baiko *et al.* [32] have shown that

$$\frac{u'}{\Gamma} = -C_M + \frac{r_T^2}{2a^2} + \sqrt{\frac{3}{\pi}} \frac{a}{2r_T} + \cdots,$$
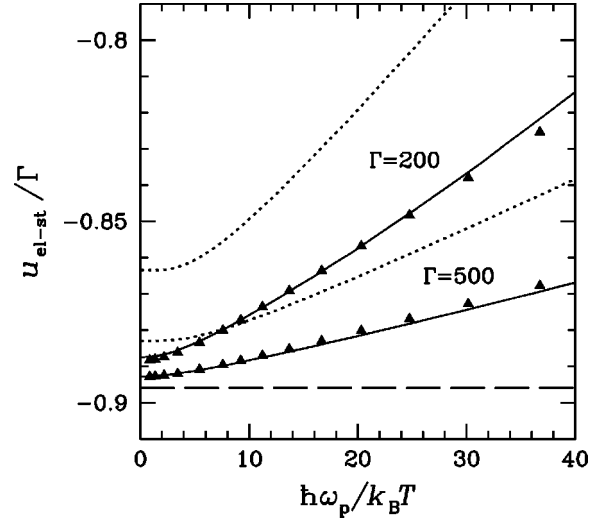

FIG. 5. Normalized electrostatic energy of a bcc Coulomb crystal calculated using the approximate structure factor given by Eq. (34) (solid lines) compared with analogous calculations with a model structure factor, Eq. (33) (dotted lines), and with accurate numerical calculations [33] (triangles). Upper curve of each type or symbol corresponds to $\Gamma = 200$ and lower one to $\Gamma = 500$. Long-dashed line displays the Madelung limit.

where the terms not explicitly written are exponentially small at large Γ. For the inelastic contribution, our model yields $u'' = u_0'' + u_1''$, where

$$u_0'' = \frac{\Gamma a}{\pi} \int_0^\infty [S_0''(k) - 1] dk = -\sqrt{\frac{3}{\pi}} \frac{\Gamma a}{2r_T}, \tag{38}$$

$$u_1'' = \frac{\Gamma a}{\pi} \int_0^{k_1} [S_1''(k) - S_0''(k)] dk$$

$$= \frac{(k_1 a)^3}{18\pi} \frac{\eta}{\tanh(\eta/2)} - \frac{\Gamma a}{\pi} \left[k_1 - \frac{\sqrt{3\pi}}{2r_T} \operatorname{erf} \frac{r_T k_1}{\sqrt{3}} \right]. \tag{39}$$

On the other hand, in the harmonic lattice approximation, $U_{el\text{-}st} = -N_i C_M (Ze)^2/a + U_v/2$, where the first term represents the energy of a perfect ionic lattice in uniform electron background, C_M being the Madelung constant (Table II), and, from the virial theorem, the second term is one-half of the vibrational energy of a harmonic crystal,

$$U_v = 3N_i k_B T \left[\left\langle \frac{\omega_\nu}{\omega_p} \frac{\eta}{e^{\eta\omega_\nu/\omega_p} - 1} \right\rangle_{ph} + \frac{\mu_1 \eta}{2} \right]. \tag{40}$$

We determine k_1 so as to recover the classical limit $u_{el\text{-}st} = -C_M \Gamma + 3/2$ at $\eta = 0$ and $\Gamma \to \infty$. This yields

$$\frac{k_1}{q_{BZ}} = \left(\frac{\mu_{-2} - 3}{\mu_{-2} - 1} \right)^{1/3} \approx 0.94. \tag{41}$$

Figure 5 shows $u_{el\text{-}st}$ calculated from Eqs. (37)–(39) for the bcc crystal at *finite* η and Γ (dot-dashed lines), compared with a calculation in which S'' is set equal to S_0'' at any k (dotted lines) and with results of numerical calculations [33].
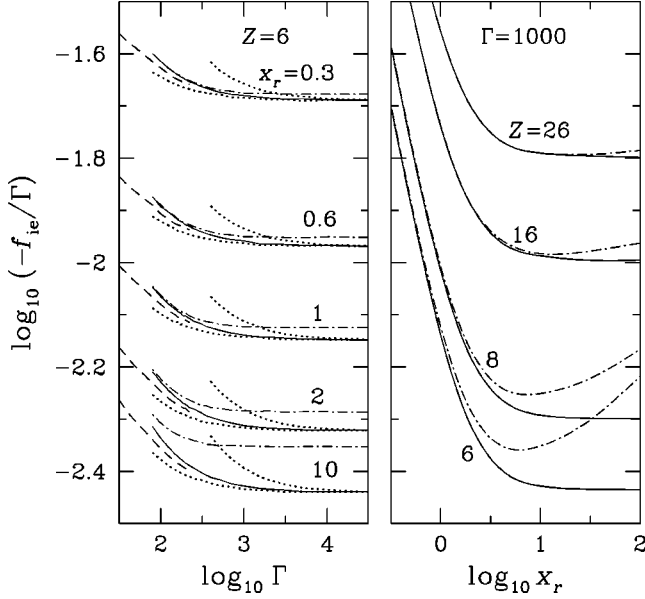
FIG. 6. Normalized polarization correction f_{ie} to the free energy of a Coulomb crystal. Left panel: $\log_{10}(-f_{ie}/\Gamma)$ against $\log_{10}\Gamma$ at $Z=6$ for several values of x_r. Right panel: $\log_{10}(-f_{ie}/\Gamma)$ against $\log_{10}x_r$ at $\Gamma=10^3$ for several values of Z. Solid lines: a classical solid; dot-dashed lines: quantum effects included. On the left panel, dotted lines show the results for the classical solid with simplified structure factors, and dashed lines show the results in a liquid.

We see that our modification of the structure factor at $k < 0.94q_{BZ}$ provides a significant improvement over the model without such modification (denoted as HL1 in Ref. [32]).

C. Results

Using Eqs. (28)–(30) and (33)–(35), we have calculated the polarization correction f_{ie} over a wide range of parameters: $80 \leq \Gamma \leq 3 \times 10^4$, $10^{-2} \leq x_r \leq 10^2$, and $1 \leq Z \leq 92$. Not all combinations of the considered parameters are physically relevant; for instance, at $Z=1$ and large x_r the ion-exchange effects neglected in our study become important. The use of such an extended set of parameters, however, delivers robustness to the fitting formula presented below.

Some results of our calculations are shown in Fig. 6. Solid lines correspond to the piecewise approximation (34) of the structure factor in the classical case ($\eta \to 0$). Dashed lines on the left panel reproduce calculations in the liquid with $S(k,\Gamma)$ from Ref. [22]. The upper and lower dotted lines at every value of x_r show, respectively, the results of calculations with the inelastic part of the structure factor replaced by S_0'' (as in the HL1 model of Ref. [32]) and by 0 (as in Refs. [4,30]). Compared to these simplified approximations, the present model provides a smaller discontinuity of f_{ie} at the freezing point (near the ends of the dashed lines). On the other hand, the divergence of the dotted curves towards smaller Γ shows that the result is still model-dependent. This model dependence disappears at $\Gamma \gtrsim 3000$, since the static-lattice contribution becomes relatively large.

In reality, at large values of Γ and small values of x_r shown in Fig. 6, the quantization of ionic vibrations becomes important. This quantization considerably modifies the struc-

TABLE III. Parameters of Eq. (42).

Lattice type	a_1	a_2	a_3	a_4	q
bcc	1.1866	0.684	17.9	41.5	0.205
fcc	1.1857	0.663	17.1	40.0	0.212

ture factor. This effect is taken into account by letting η be finite in Eqs. (27) and (35). Results of the calculations, where η was determined from Eq. (9) assuming $A=2Z$, are plotted in Fig. 6 by dot-dashed lines. The curves on the left panel become flat as η becomes large, which corresponds to an approximate proportionality $f_{ie} \propto \Gamma$. As a consequence, the polarization contribution to the specific heat, $C_{V,ie}$, goes to zero at large η (but remains one of the leading contributions, as shown below).

The numerical results can be fitted by the expression

$$f_{ie} = -f_\infty(x_r)\Gamma\{1 + A(x_r)[Q(\eta)/\Gamma]^s\}, \tag{42}$$

where

$$f_\infty(x) = a_{TF}Z^{2/3}b_1\sqrt{1+b_2/x^2},$$

$$A(x) = \frac{b_3 + a_3 x^2}{1 + b_4 x^2},$$

$$Q(\eta) = \sqrt{1+(q\eta)^2},$$

and parameters s and b_1-b_4 depend on Z:

$$s = [1 + 0.01(\ln Z)^{3/2} + 0.097Z^{-2}]^{-1},$$

$$b_1 = 1 - a_1 Z^{-0.267} + 0.27Z^{-1},$$

$$b_2 = 1 + \frac{2.25}{Z^{1/3}}\frac{1 + a_2 Z^5 + 0.222Z^6}{1 + 0.222Z^6},$$

$$b_3 = a_4/(1 + \ln Z),$$

$$b_4 = 0.395 \ln Z + 0.347Z^{-3/2}.$$

The parameter a_{TF}, related to c_{TF} in Eq. (19), is chosen so as to reproduce the Thomas-Fermi limit [23] at $Z \to \infty$: $a_{TF} = (54/175)(12/\pi)^{1/3}\alpha_f = 0.00352$. The numerical parameters a_1-a_4 and q are slightly different for bcc and fcc crystals; they are given in Table III.

For a classical crystal, an average error of the fit is 1% for all Z, x_r, and Γ, and the maximum error is 3.1% at $Z = 92$, $\Gamma \gtrsim 10^4$, and $x_r \approx 2$. In the quantum case ($\eta \neq 0$), the fit is accurate for $Z \geq 3$ only. In the range $3 \leq Z \leq 30$, an average error is 1%, and a maximum 3% occurs at $Z=3$, $\Gamma \approx 100$, and $x_r \approx 2$.

D. Discussion

The results presented in Fig. 6 indicate that, although the polarization in a Coulomb crystal is very weak, it does not vanish even at arbitrarily large Γ and x_r. As in the case of strongly coupled liquid, f_{ie} is roughly proportional to $(k_{TF}a)^2$, which tends to a finite limit at relativistic densities. The order of magnitude of the screening correction δ_{ie}
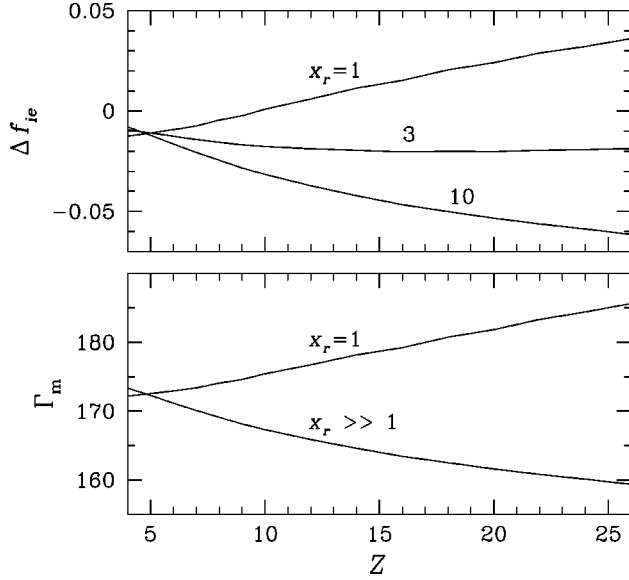
FIG. 7. Upper panel: difference between polarization corrections to the free energy in the solid and liquid phases at $\Gamma = 175, x_r = 1, 3, 10$. Lower panel: Coulomb coupling parameter at the melting point when polarization corrections are taken into account.

$= F_{ie}/F_{\text{tot}}$ for a classical Coulomb plasma at arbitrarily high densities is given by the Thomas-Fermi result [23], which is reproduced by Eq. (42) at $\Gamma \to \infty$ and $Z \to \infty$: $\delta_{ie} \approx 0.004 Z^{2/3}$. A quantitative difference of the perturbation result at finite Z from the Thomas-Fermi limit is quite noticeable, $\sim Z^{-0.3}$.

As mentioned in Sec. V A, our treatment of the screening contribution is approximate. Nevertheless, we can use these results in order to demonstrate the importance of the polarization corrections. On the upper panel of Fig. 7, the difference Δf_{ie} between f_{ie} values in the solid and liquid Coulomb plasmas at the OCP melting point $\Gamma = 175$ is plotted against Z for three values of x_r. The largest $x_r = 10$ represents virtually the ultrarelativistic limit. When compared to Fig. 2, this plot shows that Δf_{ie} is sufficiently large to affect Γ_m. This effect is shown on the lower panel of Fig. 7, where we have plotted our estimate of Γ_m at $x_r = 1$ and $x_r \gg 1$. Since Δf_{ie} remains finite at any x_r, the classical OCP value $\Gamma_m = 175$ is never exactly recovered even at arbitrarily large ρ.

Another important effect of the polarization corrections in the solid phase is that on the specific heat C_V. By differentiation of Eq. (42), we obtain

$$u_{ie} = -f_\infty \Gamma [1 + A(1 - s/Q^2)(Q/\Gamma)^s], \qquad (43)$$

$$\frac{C_{V,ie}}{N_i k_B} = f_\infty s A \left(\frac{\Gamma}{Q} \right)^{1-s} \frac{(q\eta)^2 - 1 + s}{Q^3}. \qquad (44)$$

In a classical crystal, $C_{V,ie}$ is only a small negative correction to the total $C_V \approx 3 N_i k_B$. When T decreases much below T_p, the heat capacity of an ionic crystal [29] goes to zero as $C_{V,i} \approx 1.6 N_i k_B \pi^4/(\alpha\eta)^3 \propto T^3$, whereas the ie contribution becomes positive and decreases as

$$C_{V,ie} \sim N_i k_B f_\infty s A (R_S/3q^2)^{(1-s)/2} (q\eta)^{-1} \propto T, \qquad (45)$$
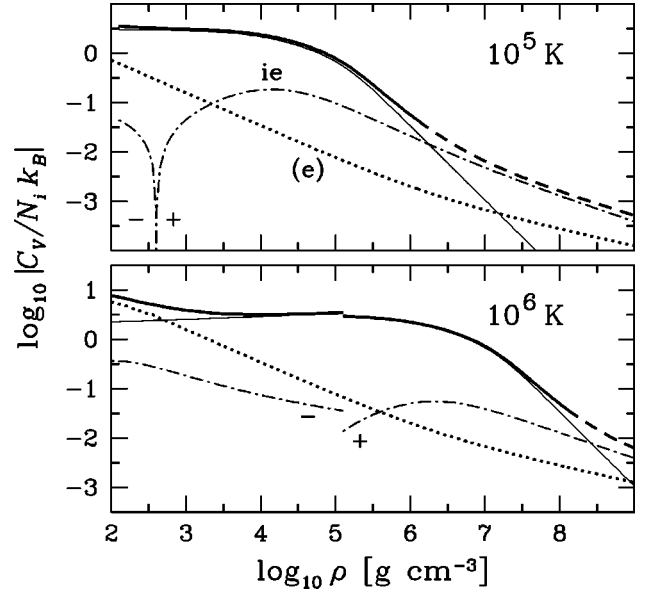

FIG. 8. Absolute values of heat capacity of carbon at high densities for two values of T. The contributions of free electrons, ionic OCP, and electron-ion interaction are shown by dotted, thin solid, and dot-dashed lines, respectively. The thick curve shows the total value. The dashed part of the latter curve corresponds to the region where the thermodynamic perturbation theory used in the calculation of $C_{V,ie}$ is not reliable.

at the same rate as the heat capacity of a strongly degenerate electron gas [11],

$$C_{V,e} \sim Z N_i (k_B T/m_e c^2) \pi^2 \sqrt{1 + x_r^2}/x_r^2. \qquad (46)$$

Equation (45), derived from the fit (42), agrees with the limiting expression at $\eta \to \infty$, which follows from Eqs. (18), (24), (33), and (27):

$$\frac{C_{V,ie}}{N_i k_B} \sim \frac{\pi^2}{\alpha^3 \eta} \left[\sum_{\mathbf{G}}{}' \frac{\varepsilon(G, x_r) - 1}{3} - \frac{2a^3}{9\pi} \int_{k_1}^\infty [\varepsilon(k, x_r) - 1] k^2 dk \right]. \qquad (47)$$

Thus $C_{V,ie}$ becomes larger than $C_{V,i}$ at sufficiently low T, which probably signifies that the thermodynamic perturbation theory is violated at this T.

The discussed effect is of anharmonic nature. Indeed, the harmonic approximation for the Hamiltonian leads to the Debye law $C_V \propto T^3$, regardless of the inclusion of the polarization correction in the force matrix. Therefore, the dependence $C_{V,ie} \propto T$ in Eqs. (45) and (47) is due to the use of the full Coulomb potential (not only its harmonic part) in the ie interaction energy, which has led to Eq. (18).

It is also noteworthy that the modification of the OCP structure factor by the quantum effects renders $C_{V,ie}$ positive. A plain extrapolation of the ie contribution from the liquid regime into the solid would be completely inappropriate, as it would result in a negative total heat capacity.

The behavior of different contributions to the heat capacity in the solid phase as a function of ρ and T is illustrated in Fig. 8. Here we consider ^{12}C at 10^5 K and 10^6 K. In the

latter case (the bottom panel), one can see also the discontinuities at the liquid-solid phase transition at $\rho \approx 10^5$ g cm^{-3}, discussed above. As in a liquid, we can safely neglect the exchange correction, which at $x_r \gg 1$ is as small as $-(\alpha_f/2\pi)C_{V,e} \sim -10^{-3}C_{V,e}$. At relatively low densities, C_V is determined mainly by the ionic contribution. As T_p becomes greater than T with increasing density, the phonon contribution to C_V freezes out rapidly, and C_V becomes determined by the degenerate electron gas, polarized by the electric field of ions.

This may have important consequences for astrophysical applications. In particular, the heat capacity of old white dwarfs, whose temperature is so low that their interiors are made of quantum Coulomb crystals [25], may be substantially influenced by the polarization effects [34].

VI. SUMMARY

We have improved analytic approximations [1] for the contributions to the free energy of a Coulomb liquid due to the ii and ie correlations. In addition, we have suggested an approximation for the ie contribution to the free energy of a Coulomb crystal.

An improvement of the ii part enables us to determine accurately the classical OCP melting point. The Coulomb coupling parameter at the phase transition is found to be $\Gamma_m \approx 175$, slightly larger than a previously determined value. An improvement of the ie part in the liquid phase yields a better precision at densities $\rho \gtrsim 10^6$ g cm^{-3}, where the electrons are relativistic. Finally, our estimates of the ie part of the free energy of a Coulomb crystal show that it is important for applications. For example, our results demonstrate that it affects the melting of a classical Coulomb crystal and may contribute appreciably to the heat capacity of a quantum crystal. Since our calculations for the Coulomb solid are based on an approximate method and performed using an approximate structure factor, the latter results can be considered as estimates only. These estimates show, however, that the polarization corrections in Coulomb crystals are not as unimportant as was often believed; they deserve to be studied further using more elaborate methods.

[1] G. Chabrier and A. Y. Potekhin, Phys. Rev. E **58**, 4941 (1998).

[2] G. Chabrier, J. Phys. (Paris) **51**, 1607 (1990).

[3] B. Jancovici, Nuovo Cimento **25**, 428 (1962).

[4] D. A. Baiko, A. D. Kaminker, A. Y. Potekhin, and D. G. Yakovlev, Phys. Rev. Lett. **81**, 5556 (1998).

[5] S. L. Shapiro and S. A. Teukolsky, *Black Holes, White Dwarfs, and Neutron Stars: The Physics of Compact Objects* (Wiley, New York, 1983).

[6] H. E. DeWitt and W. Slattery, Contrib. Plasma Phys. **39**, 97 (1999).

[7] J. M. Caillol, J. Chem. Phys. **111**, 6538 (1999).

[8] M. D. Jones and D. M. Ceperley, Phys. Rev. Lett. **76**, 4572 (1996).

[9] S. Ichimaru, H. Iyetomi, and S. Tanaka, Phys. Rep. **149**, 91 (1987).

[10] W. Stolzmann and T. Blöcker, Astron. Astrophys. **314**, 1024 (1996).

[11] D. G. Yakovlev and D. A. Shalybkov, Astrophys. Space Phys. Rev. **7**, 311 (1989).

[12] R. Abe, Prog. Theor. Phys. **21**, 475 (1959).

[13] E. G. D. Cohen and T. J. Murphy, Phys. Fluids **12**, 1404 (1969).

[14] H. E. DeWitt (private communication).

[15] T. Kahlbaum, in *Physics of Strongly Coupled Plasmas*, edited by W. D. Kraeft and M. Schlanges (World Scientific, Singapore, 1996), p. 99.

[16] W. Stolzmann and T. Blöcker, Contrib. Plasma Phys. **39**, 105 (1999).

[17] H. Nagara, Y. Nagata, and T. Nakamura, Phys. Rev. A **36**, 1859 (1987).

[18] D. H. E. Dubin, Phys. Rev. A **42**, 4972 (1990).

[19] W. L. Slattery, G. D. Doolen, and H. E. DeWitt, Phys. Rev. A **26**, 2255 (1982).

[20] R. T. Farouki and S. Hamaguchi, Phys. Rev. E **47**, 4330 (1993).

[21] S. Galam and J. P. Hansen, Phys. Rev. A **14**, 816 (1976).

[22] D. A. Young, E. M. Corey, and H. E. DeWitt, Phys. Rev. A **44**, 6508 (1991).

[23] E. E. Salpeter, Astrophys. J. **134**, 669 (1961).

[24] A. Y. Potekhin, G. Chabrier, and D. G. Yakovlev, Astron. Astrophys. **323**, 415 (1997).

[25] L. Segretain, G. Chabrier, M. Hernanz, E. García-Berro, J. Isern, and R. Mochkovitch, Astrophys. J. **434**, 641 (1994).

[26] E. L. Pollock and J. P. Hansen, Phys. Rev. A **8**, 3110 (1973).

[27] C. Kittel, *Quantum Theory of Solids* (Wiley, New York, 1963).

[28] G. Chabrier, N. W. Ashcroft, and H. E. DeWitt, Nature (London) **360**, 48 (1992).

[29] G. Chabrier, Astrophys. J. **414**, 695 (1993).

[30] A. Y. Potekhin, D. A. Baiko, P. Haensel, and D. G. Yakovlev, Astron. Astrophys. **346**, 345 (1999).

[31] P. Vieillefosse and J. P. Hansen, Phys. Rev. A **12**, 1106 (1975).

[32] D. A. Baiko, D. G. Yakovlev, H. E. DeWitt, and W. L. Slattery, Phys. Rev. E **61**, 1912 (2000).

[33] D. A. Baiko, Ph.D. thesis, Ioffe Phys.-Tech. Institute, St. Petersburg, 2000.

[34] G. Chabrier, P. Brassard, G. Fontaine, and D. Saumon, Astrophys. J. (to be published).